ENGINEERING TRANSACTIONS • *Engng. Trans.* • **53**, 1, 55–68, 2005
Polish Academy of Sciences • Institute of Fundamental Technological Research
10.24423/engtrans.432.2005

NUMERICAL EVALUATION OF DELAMINATION ON MODE II IN GLASS FIBER REINFORCED COMPOSITES[1)]

M. R. Khoshravan, M. Monir Vaghefi

Mechanical Engineering Department,
Faculty of Engineering,
University of Tabriz, Tabriz, Iran
e-mail: rkhosh@tabrizu.ac.ir

In this paper, delamination of Mode II in a stratified glass fiber-epoxy resin under static loading is investigated. From the results obtained by the finite element method, using the criteria of Irwin–Kies and other theories of elasticity, the strain energy release rate is evaluated. The obtained numerical results are compared with known experimental and theoretical results. Considering local effects, such as fiber bridging in the finite element program, the scatter between experimental and numerical results is evaluated. The specimen is an ENF (End-Notched Flexure) beam and finite element analysis is carried out using the ANSYS software.

1. Introduction

Since the composite materials have a high strength and low weight, they are useful for all engineering structures. The use of these materials in the structures of aeronautic, marine vehicles, cars and the likes, is ever increasing and has found its place in other fields of industry. Further information on destruction and rupture of these materials has a special importance.

The rupture of a composite material, because of the variety of the mechanisms used in the destruction of structure, is very complicated. Figure 1 shows a variety of possibilities of destruction.

In multilayer composites another phenomenon is added to the mechanisms of failure, which is delamination of the layers. In the mechanism of delamination which is analogous to the crack growth in the isotropic materials, all the possibilities of rupture shown in Fig. 1 exist.

The mechanical behaviour of thermoset matrix composite materials is similar to the brittle materials. So the plastic zone at the tip of crack is very small and in analyses using finite element method, the plasticity of that zone is not considered.

[1)]Paper presented at the 34-th Solids Mechanics Conference, September 2–7, 2002, Zakopane.

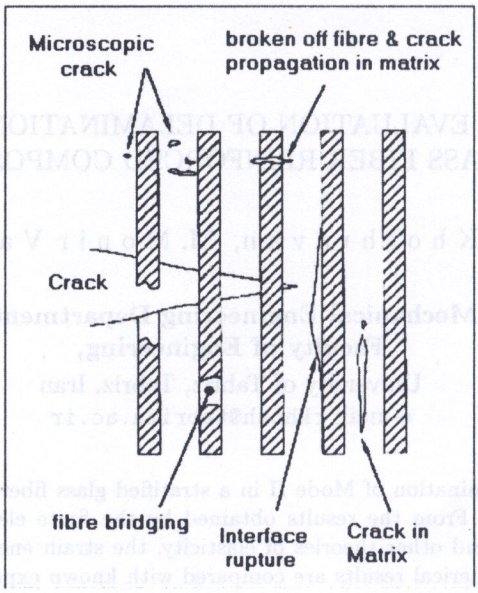

FIG. 1. The type of rupture in composite structure.

In the second mode of rupture, as shown in Fig. 2, the direction of delamination is the same as the one of the applied load direction. Rupture of this mode is the result of shear, and during delamination, the faces of the crack slide on each other.

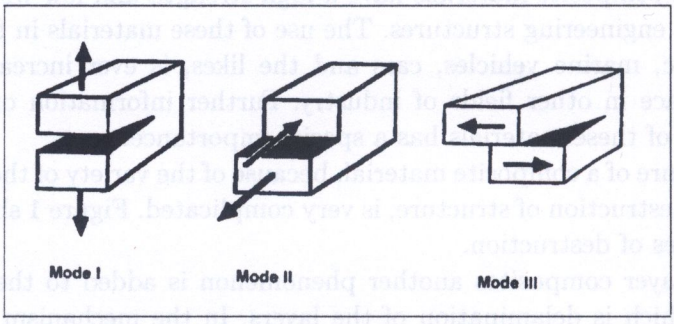

FIG. 2. Different kinds of crack mode.

2. ENF SPECIMEN

This specimen is used to study the delamination in Mode II. As shown in Fig. 3, it is a beam subjected to three-point bending, and load P is applied

in the middle of the beam. We distinguish: a zone without precrack, the lower layers (below the precrack), the upper layers (above the precrack). When the load is applied, the upper layers are loaded in compression and lower layers in tension. If the applied load exceeds the critical value, these compressive stresses and tensile stresses lead to the shear at the end of the crack and delamination in Mode II occurs.

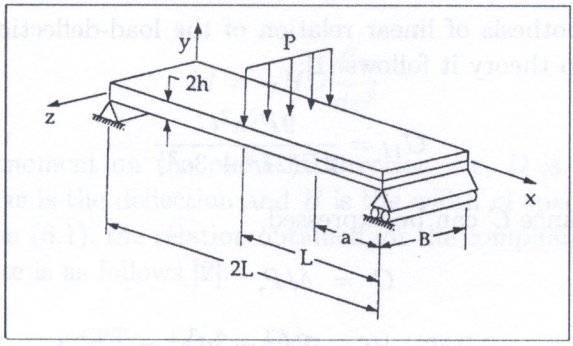

FIG. 3. ENF specimen.

The properties and dimensions of the specimen which is used in our finite element method, are shown in the Table 1. This type of specimen is used by Money to measure experimentally the strain energy release rate [1].

Table 1. Properties and geometry of the specimen.

Geometry	Properties
$L = 50$ mm	$E_x = 40$ GPa
$h = 1.5$ mm	$E_y = E_z = 10.5$ GPa
$B = 25$ mm	$\upsilon_{xy} = 0.3$
$a = 10$ mm	$\upsilon_{xz} = \upsilon_{yz} = 0.078$
$LT = 120$ mm	

3. CRITERIA OF STRAIN ENERGY RELEASE RATE

In this criterion, when the strain energy applied to a composite material with precrack reaches the critical value, delamination occurs. The Irwin–Kies theory to evaluate the strain energy release rate [2] is as follows:

$$G = \frac{P^2}{2B}\frac{\partial C}{\partial a}, \tag{3.1}$$

where $C = \delta/p$ is the compliance of the specimen. P is the applied load, B the width of specimen, a the crack length, and δ, in the relation for the compliance

represents the deflection of specimen in the point of load application. If G reaches its critical value, delamination occurs.

There are different methods to measure G_{II} of ENF specimen. Some of them are explained below.

4. Beam theory

With the hypothesis of linear relation of the load-deflection relationship of G, from the beam theory it follows [1]:

$$G_{II} = \frac{9P^2a^2C}{2B(2L^3 + 3a^3)}. \tag{4.1}$$

Here, the compliance C can be expressed,

$$C = \delta/P, \tag{4.2}$$

$$C = \frac{2L^3 + 3a^3}{8EBh^3}. \tag{4.3}$$

Relation (4.3) is obtained from the beam theory, by substituting relations (4.2) and (4.3) in relation (4.1). Thus we obtain:

$$G_{II}^{\mathrm{CBT}} = \frac{9Pa^2\delta}{2B(2L^3 + 3a^3)}, \tag{4.4}$$

$$G_{II}^{\mathrm{BT}} = \frac{9P^2a^2}{16EB^2h^3} \tag{4.5}$$

(BT: Beam Theory, CBT: Compliance Beam Theory).

Physical properties of materials (such as the Young modulus: E), are known with some percent of error, so relationship (4.4), in which physical indicators of the material do not appear explicitly, has higher precision than relation (4.5).

5. Calibration method

In this experimental method, by measuring the crack length, the critical load (which leads to crack growth) and the deflection of specimen (δ), the compliance is calculated. This experiment is carried out on the test bars with different initial crack lengths and the results are demonstrated by a curve of compliance versus the crack length.

In this method, the strain energy release rate is evaluated as follows:

$$G_{II} = \frac{P^2}{2B}\frac{\Delta C}{\Delta a}. \tag{5.1}$$

Here $\Delta C/\Delta a$ is the slope of the curve of compliance versus crack length (obtained from the experiment).

6. Classical theory of plates

The general relationship for plates is:

$$M = -BD\frac{d^2w}{dx^2}. \tag{6.1}$$

Here, M is the moment on the plane in direction $+x$, D is the coefficient of bending rigidity, w is the deflection and B is the width of specimen.

Using equation (6.1), the relation obtained for the compliance and the strain energy release rate is as follows [2]:

$$C^{\mathrm{CPT}} = \left[4L^3 + a^3(R-2)\right]/(24BD), \tag{6.2}$$

$$\mathrm{G}_{II}^{\mathrm{CPT}} = \frac{3P\delta a^2}{2B} \cdot \frac{(R-2)}{\left[4L^3 + a^3(R-2)\right]}, \tag{6.3}$$

$$R = D/D_1, \qquad D = 2E_{11}h^3/3.$$

Here, δ is the deflection of plate and D_1 is the bending rigidity of the crack zone. In unidirectional test bars R is usually equal to 8. In terms of R, the relations (4.4) and (6.3) become identical. The kind of supports of the ENF specimen influences also the value of R. A roller support decreases R and a corner-shaped support increases it [3].

7. Shear deformable plate theory

The eliminated part of the equation of the classical theory of plates which contains the effect of variation of shear form of plates, influences the strain energy release rate. Using the beam theory of Timoshenko, relation (6.1) is corrected in order to take into account the effect of the shear deformation and strain energy release rate. Thus the relation becomes:

$$G_{II}^{\mathrm{SPT}} = G_{II}^{\mathrm{CPT}}\left[1 + \frac{9D}{5a^2hG_{13}(R-2)}\right]. \tag{7.1}$$

G_{13} is the shear modulus in plane $(X - Z)$ (Fig. 3).

8. Finite element model of the ENF specimen

For two-dimensional (2D) modeling, we have used the element of four corners with 8 nodes and element of three corners with 6 nodes. As the width of specimen is higher than its thickness, the problem is studied in plane strain state. As the dimension of the zone of stress concentration is lower than the dimensions of the rest of specimen, only a small zone around the tip of the crack is grid generated with a high concentration. The type of element and the type of mesh generation lead to the singularity of stress and strain at the tip of the crack (Fig. 4).

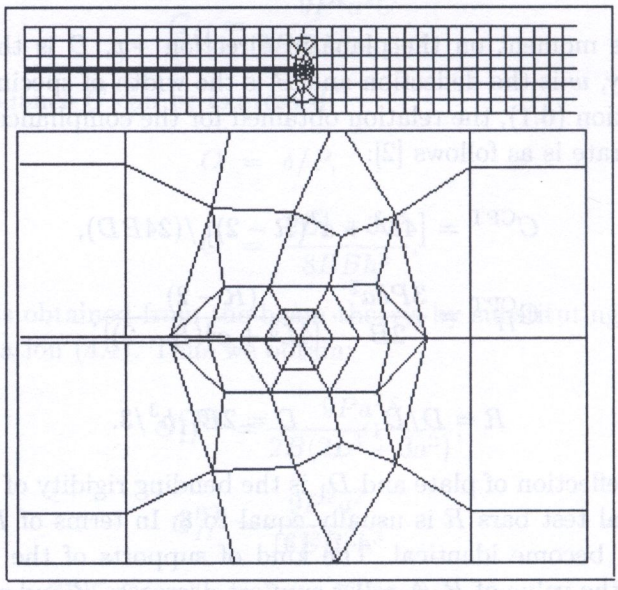

Fig. 4. Meshing and elements in crack tip.

Also, in the point of load application and location of supports, we have assumed a high concentration of grids.

In a real specimen, the supports and the point of load application have the shape of a roller, so there is a surface of contact instead of a point of contact. To establish this support condition, we have limited the liberty of displacement of the nodes situated in the vicinity of the load application points. The kind of load application is based on the order of displacement of the nodes in the middle of specimen.

In the three-dimensional (3D) specimen, we have used an element of six faces with 20 nodes and an element of 5 faces with 15 nodes.

The type of grids and boundary conditions are also taken as a 2D specimen.

9. Rupture at the tip of the crack

Analyzing the specimen by using the finite element method, different stresses are calculated at the end of crack. Using one of the rupture criteria in composite materials and the obtained stresses at the end of the crack, the strain energy release rate of the specimen for delamination is evaluated. As the plastic zone at the end of the crack is very little, we consider only an elastic rupture at the end of the crack.

10. Theory of Tsai–Hill

$$\left(\frac{\sigma_x}{X}\right)^2 - \frac{\sigma_x \sigma_y}{X^2} + \left(\frac{\sigma_y}{Y}\right)^2 + \left(\frac{\tau_{xy}}{S}\right)^2 = 1. \tag{10.1}$$

This criterion is obtained from development of the von Mises theory. If the stresses in a test satisfy the relation (10.1), the test bar will be at the beginning of rupture. X, Y are the yield stresses in directions x, y and S is the shear yield stress on the xy plane.

11. Theory of Tsai–Wu

According to this theory, if the stresses increase to the extent that the relation (11.1) becomes true, the test bar will be at the beginning of rupture.

$$\frac{\sigma_x^2}{X_t X_c} + \frac{C_{xy}\sigma_x\sigma_y}{\sqrt{X_t X_c Y_c Y_t}} + \frac{\sigma_y^2}{Y_t Y_c} + \frac{\tau_{xy}^2}{S^2} + \left(\frac{1}{X_t} - \frac{1}{X_c}\right)\sigma_x + \left(\frac{1}{Y_t} - \frac{1}{Y_c}\right)\sigma_y = 1. \tag{11.1}$$

The index t means tension, and index c means compression. C_{xy} is the coefficient in the plane xy, which is equal to (-1) for a unidirectional composite [4].

In the finite element method using the above theory, the critical load (P_c) and deflection (δ_c), for which the stresses at the tip of the crack reach their critical values (limit of rupture), are computed. Repeating this analysis for different initial crack lengths, we obtain the compliance as a function of the crack length. Using the general relation of strain energy release rate, the value of G_{II} as a function of crack length is obtained.

12. Distribution of strain energy release rate in front of the crack

In the effect of load application to the test bar, the lower plane of the upper half-beam (the half-beam situated above the crack) is contracted in longitudinal direction.

As the effect of transversal strain of the width, this lower plane expands in the half-beam situated below the crack (Fig. 5). Expansion and contraction of the width of specimen in the planes of crack increase locally the strain energy release rate in the two edges in front of the crack. So, the total strain energy release rate at the end lines the crack, is a sum of G_{II} and G_{III}.

$$G_t = G_{II} + G_{III}. \tag{12.1}$$

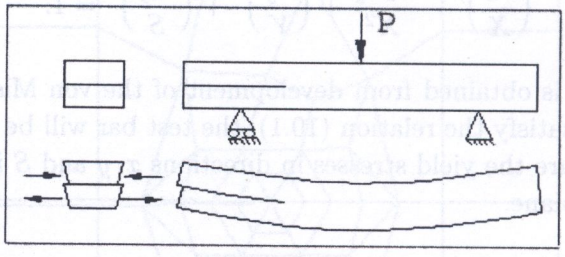

Fig. 5. Deformation of width and length of crack zone in Mode II.

The curve of Fig. 6 shows the distribution of strain energy release rate according to Mode II and III in direction of the width of the specimen normalized

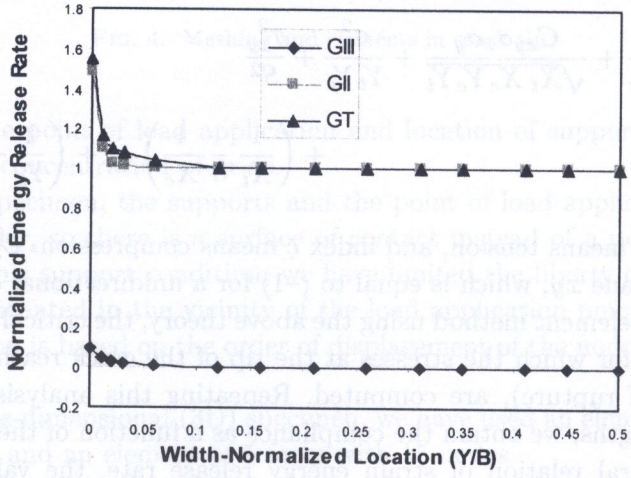

Fig. 6. Energy release rate distribution in width crack tip.

in relation to G_{II}. For unidirectional composites, this distribution of G, relative to the center of the width of the test bar is symmetric [5]. In the 2D specimen, we do not observe this effect. So this effect is called three-dimensional, 3D effect.

13. The effect of fiber bridging

The effect of fiber bridging from the matrix between the two faces of the crack should be taken into account in the analysis of delamination (Fig. 7). The area in which we observe this phenomenon, is a small zone in the left-hand part of the crack. During the crack growth, this zone follows the delamination. The existence of this zone increases the strain energy release rate, because after rupture occuring at the end of the crack, a part of energy is used to pull out the fiber from the matrix. This effect (fiber bridging) operates like the plastic zone at the end of the crack in isotropic materials. Thus, the total strain energy release rate is the sum of strain energy release rate of crack growth (theory of Irwin–Kies) G_m and the strain energy release rate, resulting from fiber bridging of the matrix, G_p.

$$G_t = G_p + G_m. \tag{13.1}$$

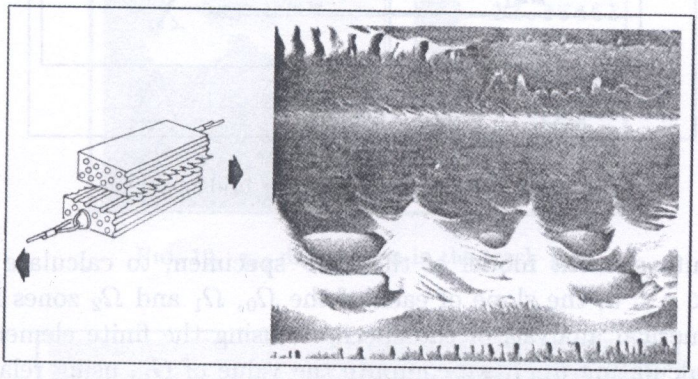

FIG. 7. Fiber-bridging effect.

In the theoritical analysis, at the mentioned zone, in order to take into account the fiber bridging from the matrix, the load in interface of crack is as follows [6]:

$$\begin{cases} f(x) = f_{IIc} - k\Delta u(x) & \Delta u(x) \leq \Delta u_c, \\ f(x) = 0 & \Delta u(x) \geq \Delta u_c, \end{cases} \tag{13.2}$$

$$\Delta u(x) = \frac{h}{4}\left[\frac{dw_1(x)}{dx} - \frac{dw_2(x)}{dx}\right] - \frac{h}{8}\frac{dw_0(a)}{dx}.$$

Here f_{IIC} is the critical value of $f(x)$, which depends on the material and its properties. K is the constant coefficient and $u(x)$ is the difference between slopes of the upper layers and lower layers of the crack. Δu_c is the initial value of Δu_x, for which the crack starts to develop. w_0, w_1 and w_2 are the deflections of each zone (Fig. 8). The strain energy release rate (G_p) is obtained from the following relation:

$$\frac{1}{2}\int_a^m f_{IIC} B \frac{d}{da}(\Delta u(x)).dx, \tag{13.3}$$

in which m is the distance from the end of bridging zone of the fiber of the matrix to the left edge of the specimen (Fig. 8).

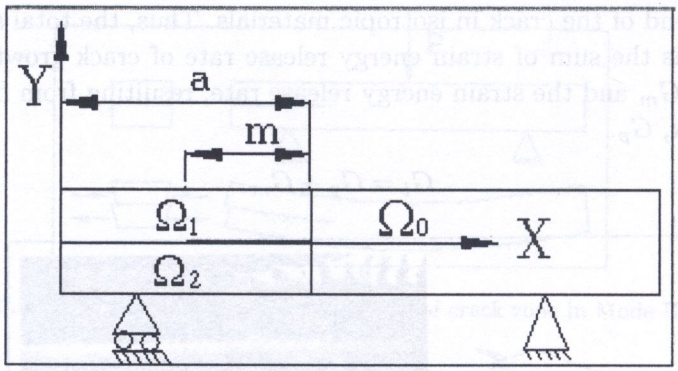

FIG. 8. ENF specimen with fiber bridging zone.

In the finite element model of the ENF specimen, to calculate G_p at the distance $m < x < a$, the slope of each of the Ω_0, Ω_1 and Ω_2 zones is obtained from the numerical analysis of the specimen using the finite element method: then, after calculating $u(x)$, we compute the value of G_p, using relation (13.3) by numerical integration method.

14. RESULTS

Figures 9, 10 and 11 show the stress distribution σ_x, τ_{xy} and σ_y in crack zones. For different initial crack lengths, the type of the stress distribution in crack zone will preserve its shape. In Fig. 12, the curve of strain energy release rate obtained by means of the beam theory, classical plates theory of the shear deformation theory and numerical results using the finite element method, are shown. The values of critical load P_c and maximum deflection δ_c are obtained from the experimental result [7] used in different theories.

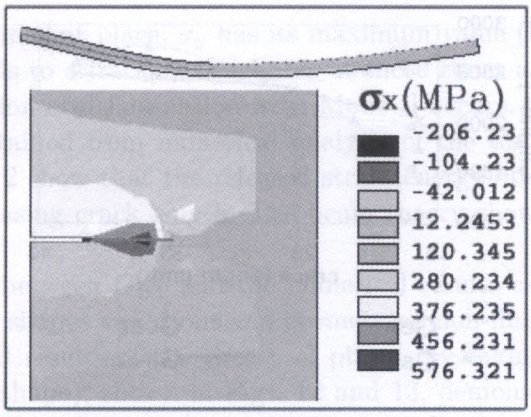

FIG. 9. σ_x distribution in the crack tip.

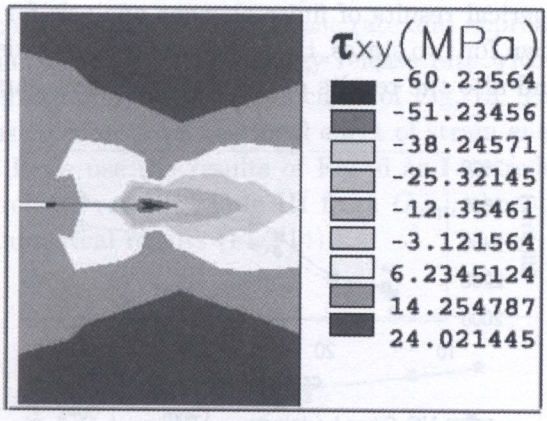

FIG. 10. τ_{xy} distribution in the crack tip.

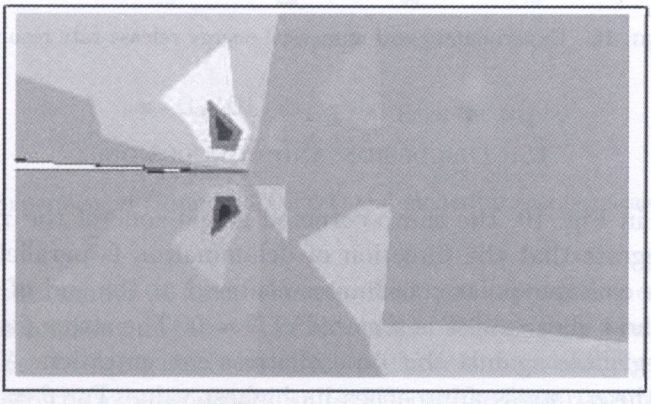

FIG. 11. σ_y distribution in the crack tip.

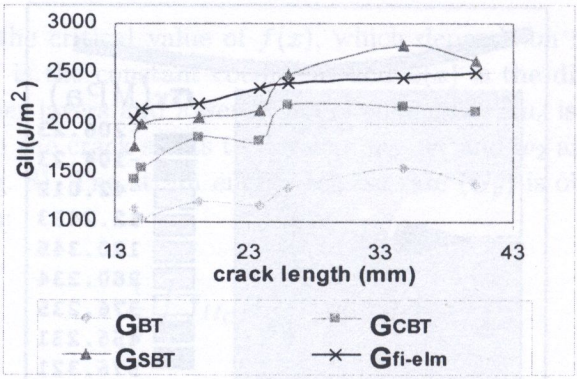

FIG. 12. Theoretical and numerical energy release rate result.

In Fig. 13, numerical results of finite element analysis for the strain energy release rate are shown for two states, the existence and non-existence of the effect of fiber bridging and also the results of calibration of test bars (G_{exp}).

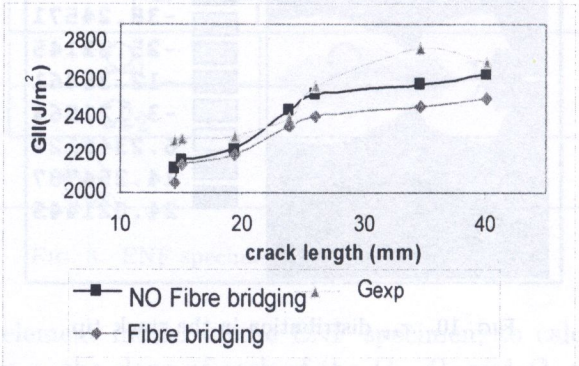

FIG. 13. Experimental and numerical energy release rate result.

15. DISCUSSION AND CONCLUSION

As we see in Fig. 10, the sharp-cornered shape zone of the τ_{xy} stress concentration suggests that the direction of delamination is parallel to the crack surfaces. If we consider polar coordinates centered at the end of the crack, for $r = 0$, the highest shear stress is situated at $\theta = 0$. The stress distribution in y direction is negligible against this type of stress concentration. Also in vicinity of the crack, the σ_y stress approaches its highest value. For $\theta = 90°$, at a distance from the end of the crack, we reach a low quantity in distribution of shear

stress and exactly in that place, σ_y has its maximum value (Fig. 11). This type of distribution leads to a fracture toughness at those zones and that is why the local cracks deviation of delamination from Mode II occurs.

The results obtained from numerical analysis of the test bars (using finite elements) in Fig. 12 show that the released strain energy does not increase significantly for increasing crack length. The beam theory shows also this kind of behaviour.

The difference between G_{BT} and the numerical results can be explained by the effects of shear shapes variations and geometrical non-linearities. The experimental results and results of the theory of plates (by taking into account the variation of shear shape), shown in Figs. 12 and 13, demonstrates the increase of strain energy release rate in terms of crack growth. Considering the separation zone of the fiber from layers, we see this increasing in numerical results using the finite element method (Fig. 13). These results show that fiber bridging effect influences the strain energy release rate and approaches the numerical results of experiments. G_{exp} (strain energy release rate with calibration of test bars) reaches its maximum values in the curve of Fig. 13. The error relevant to this method seems to come from the local effect of strain energy release rate on Mode III (G_{III}). If we use the results of Fig. 6 and we reduce the local value of strain energy release rate in Mode III from G_{exp}, the obtained results will approach to the numerical results (Fig. 14).

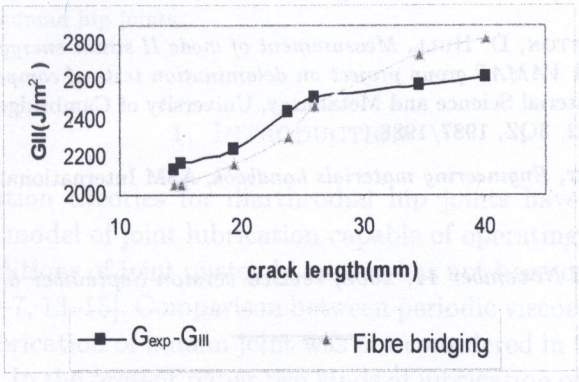

FIG. 14. Experimental (without 3D effect) and numerical energy release rate result.

Though, this model of finite element does not represent a complete model of rupture mechanisms at the end of the crack. Taking into consideration some effects like fiber bridging and the effect of three-dimensionality, the numerical results approach the experimental results. Effects like fiber rupture in the matrix, the type of supports of test bars, the friction between surfaces of crack and

the likes, which need a statistical analysis, should also enter the mechanisms of delamination and their effects on the strain energy release rate should be evaluated.

References

1. M. W. Money, *Measurement of mode I and mode II strain energy release rates*, National Physical Laboratory, NPL Report DMA(A) 178, March 1989.
2. B. D. Davidson, R. Kruger, M. Konig, *3-Dimensional analysis and resulting design recommendation for unidirectional and multidirectional end-notched-flexure tests*, Journal of Composite Material, **29**, 2108–2133, 1995.
3. B. D. Davidson, C. S. Altonen, J. J. Polaha, *Effect of stacking sequence delamination toughness and delamination growth behavior in composite end-notched-flexure specimens*, Composite Materials: Testing and Design (Vol. 12), ASTM STP 1274, C. R. Saff and R. B. Deo [Eds.], ASTM, 393–413, 1996.
4. Tsai Stephen, W. Hahn, H. Thomas, *Introduction to composite materials*, Sec. 7.2, Technomic Publishing Company, 1980.
5. B. D. Davidson, R. Kruger, M. Konig, *Effect of stacking of sequence on energy release rate distribution in multilayer DCB and ENF specimens*, Submitted to Engineering Fracture Mechanics, Syracuse University Department of Mechanical, Aerospace and Manufacturing Engineering Technical Report Number 95–101, 1995.
6. L. Daridon, B. Cochelin, M. Potier Ferry, *Delamination and fiber bridging modeling in composite samples*, University de Metz-IIe du Sauley 57045 Metz–Cedex 01, France, 1995.
7. W. R. Broughton, D. Hull, *Measurement of mode II strain energy release rates using the ENF test. A VAMAS group project on delamination tests of composite materials*, Department of Material Science and Metallurgy, University of Cambridge, Pembroke Street, Cambridge, CB2, 3QZ, 1987/1988.
8. T. J. Reinhart, *Engineering materials handbook*, ASM International, **1**, 788, 1987.

Received November 11, 2002; revised version September 6, 2004.